

Texture evolution in an Al-8Zn alloy during ECAP and post-ECAP isothermal annealing

Hailong Jia, Yanjun Li*

Department of Materials Science and Engineering, Norwegian University of Science and Technology (NTNU),
7491 Trondheim Norway

***Corresponding author:** Yanjun Li, Department of Materials Science and Engineering, Norwegian University of Science and Technology (NTNU), Trondheim 7491, Norway.

E-mail address: yanjun.li@ntnu.no (Y.J. Li)

Abstract

In this work, the texture evolution of an Al-8 wt.% Zn alloy during equal channel angular pressing (ECAP) and post-ECAP isothermal annealing was systematically investigated by electron backscatter diffraction (EBSD). Special attention is paid to the influence of static recovery and recrystallization on ECAP texture. After 1 pass of ECAP, the sample shows a texture similar to the ideal shear texture. Specifically, during deformation, the less deformed coarse grains rotate towards close to ideal ECAP texture orientations. With increasing ECAP passes to 5, the main texture component can still be depicted by fibers f1-f3. However, fading of the f1, f2 and f3 fibers occurs, resulting in less completed f1-f3 fibers. The weakening of ECAP texture with increasing deformation strain is attributed to continuous dynamic recrystallization (CDRX). Static recovery and recrystallization during post-ECAP isothermal annealing have a limited influence on the ECAP texture.

Keywords: Aluminium alloy; ECAP; Microstructural evolution; Texture evolution; Annealing

1. Introduction

Al-Zn binary system is the base for numerous industrial alloys due to a good combination of physical, mechanical and superplastic properties together with good abrasion and wear resistance [1-3]. At room temperature (RT), Zn has a relatively high solid solubility in Al, ~0.85 at.% (~2.0 wt.% Zn) [4]. However, the mechanical properties of binary Al-Zn alloys, such as tensile strength, are inadequate for some structural applications, which need to be further improved. One of the most effective ways is by adding alloying elements, such as Cu and Si [5]. Another one is severe plastic

deformation (SPD), which can be utilized to fabricate ultrafine grained (UFG) Al-Zn alloys with enhanced strength.

Among various SPD techniques, equal channel angular pressing (ECAP) [6-11] is especially promising because it can be scaled-up to produce bulk UFG materials. The microstructure and texture of materials can be significantly changed by the plastic deformation induced by ECAP. Studies on ECAP texture are necessary since it can help to understand the anisotropy in physical and mechanical properties of materials. In comparison to the extensive studies on the evolution of deformation structures and mechanical properties, the texture evolution during ECAP has not been paid enough attention. In terms of FCC materials, the previous studies on ECAP texture evolution have mainly focused on pure Al [12-20] and Cu [12, 21-25], with limited studies on the texture evolution of high alloyed metals [26-30]. In the work [28], in spite of the ECAP textures of different Al alloys (1050, 5083, 6082 and 7010) have been investigated, but only after one pass of ECAP. In general, the evolution of microstructure and texture during ECAP has been studied separately and most efforts have been made in investigating the macro-texture evolution during ECAP using X-ray measurement [17, 29] or neutron diffraction [21], whereas the correlation between the microstructure and the ECAP texture are not shown. In addition, most studies using route Bc are on ECAP textures after even-numbered passes, while odd-pass ECAP textures still need to be examined.

The initial texture [31], die angle [32, 33], route [33] and pass number of ECAP [34] have been shown to play some role in the formation of ECAP texture. The textures developed after 1 pass of ECAP are found to be similar to the simple shear texture [14, 32, 35-38], such as the textures after torsion deformation. Deformation textures after multiple ECAP passes depend on the ECAP route. In route A (no rotation of billet around the ED axis) and route C (the billet is rotated 180° around the ED axis), monoclinic symmetry of the first-pass ECAP texture is found to be retained [21]. In contrast, the subsequent ECAP passes in route Bc (rotation of the billet around the ED axis by 90°) result in variation of orientations and densities of the main texture components [21]. For commercial purity Al deformed after multi-pass ECAP, it has been found that compared to route Bc, the texture strength developed in route C is higher up to four passes [20].

So far, ECAP has been applied to some Al-Zn alloys with eutectic [39], eutectoid [40] and monotectoid compositions [41], whereas there appears to be a lack of investigations on the texture evolution of binary Al-Zn alloys containing less than 10 wt.% Zn during large number of ECAP passes. In addition to ECAP route and number of passes, annealing is expected to be another factor that can influence the formation of microstructures and textures. This is because annealing can modify the deformation texture, such as rolling textures. At the same time, for potential forming applications in aerospace industries, annealing on the UFG Al-Zn alloys is necessary to improve the formability. However, the influence of post-ECAP annealing on ECAP texture evolution [18, 22] is still lacking, thus systematic investigations need to be conducted on the concomitant development of microstructure and texture during post-ECAP annealing. Therefore, in the present work, in addition to the formation of ECAP texture in the binary Al-8 wt.% Zn alloy, the influence of post-ECAP isothermal annealing (recovery and full completion of static recrystallization) on the evolution of microstructure and texture have been studied.

2. Experimental

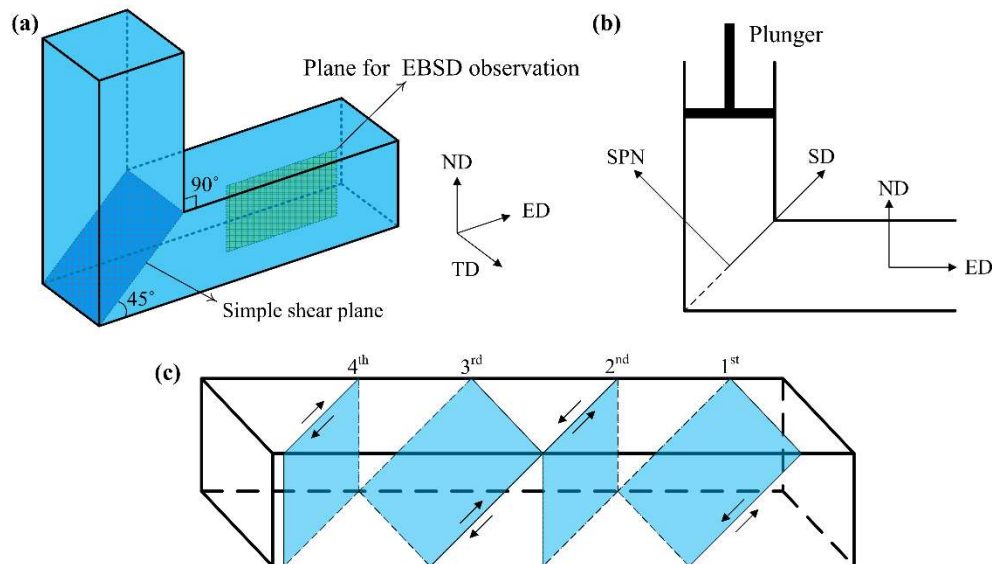


Fig. 1. (a) Schematic illustration of the 90° ECAP die and the plane for EBSD observation, (b) sketch of the ECAP die, showing the shear direction (SD) and shear plane normal (SPN), and (c) macroscopic shear patterns for consecutive passes using route Bc. ND, TD and ED are abbreviations for the normal, transverse and extrusion directions, respectively.

In the present work, the Al-8 wt.% Zn ingot was made by melting Al and Zn, both of which are in commercial purity. As shown in our previous work [42], in the as-cast state, no Zn precipitates can be observed in the Al matrix, which indicates that nearly all the Zn content is in the Al solid solution.

The as-cast ingots were machined into bars with a square cross-section of 19.5 mm × 19.5 mm and a length of 100 mm. Afterwards, well-lubricated bars were deformed repetitively by a 90° ECAP die (Fig. 1(a)) via route Bc at RT. The ECAP bars were subjected to 1, 3 and 5 passes, with an equivalent strain of about 1.0 per pass [10]. Fig. 1 includes coordinate axes of ECAP, showing that the ECAP bars exit the ECAP die along the extrusion direction (ED) axis. Route Bc means that the ECAP bar is rotated by 90° in the same sense between each pass with respect to the ED axis. The shear direction (SD) and shear plane normal (SPN) are defined in Fig. 1(b).

Post-ECAP annealing was conducted at 200 °C (oil furnace) and 350 °C (salt bath) for various times, followed by water quenching. Samples for electron backscattered diffraction (EBSD) observation were cut from the middle part of as-deformed bars (Fig. 1(a)), where the deformation structure is more uniform. Full details of the preparation of EBSD samples is the same as that in our previous work [8]. EBSD was performed on the longitudinal section (ND-ED plane) using a field emission gun SEM (Hitachi SU-6600), equipped with a Nordif EBSD detector. The texture analysis has been carried out by pole figures and the orientation distribution function (ODF) plots, both of which were obtained using the TSL OIM software, based on the orientation data collected from large areas of ~380 μm × 380 μm by EBSD. The ODF plots were calculated using the harmonic method with a series expansion of 16.

3. Results and discussion

3.1. Formation of texture during ECAP

Microstructures of the as-cast and as-ECAPed Al-8Zn alloy, as well as their corresponding pole figures are shown in Fig. 2. The average grain size of the as-cast Al-8Zn alloy was measured to be ~50 μm. The microstructural evolution during ECAP deformation has been fully presented in our previous work [42], in which the mechanism for the formation of equiaxed ultrafine grains is clarified to be continuous dynamic recrystallization (CDRX) [42]. As indicated in Fig. 2(d₁), after 5 passes of

ECAP, the average grain size is reduced down to $\sim 0.9 \mu\text{m}$. It is smaller than the steady grain size ($\sim 1.3 \mu\text{m}$) of high purity (99.99%) Al deformed by ECAP [43] while larger than the steady grain size ($\sim 0.27 \mu\text{m}$) of the Al-3 wt.% Mg alloy [43] (with similar atomic content of additional atoms to the Al-8 wt.% Zn alloy). This implies that the Zn element is less effective in refining grains than Mg.

For FCC materials, the orientations of main simple shear texture components are found to distribute along two fibers: the A-type $\{h k l\}\langle 1 1 0 \rangle$ fiber (or $\langle 1 1 0 \rangle$ -fiber in short) and the B-type $\{1 1 1\}\langle uvw \rangle$ fiber (or $\{1 1 1\}$ -fiber in short) [44], where the notation refers to $\{\text{planes} \parallel \text{SP}\}\langle \text{directions} \parallel \text{SD} \rangle$. Usually, ECAP textures are studied in the coordinate system defined by the billet reference axes, which can be related to the shear reference axes by a rotation around the TD axis, for example, 45° in a 90° ECAP die. Based on the simple shear texture, the two ECAP texture fibers can be designated as $\{1 1 1\}_\theta\langle uvw \rangle$ and $\{h k l\}\langle 110 \rangle_\theta$, respectively [21].

As can be seen from the $(1 1 0)$ and $(1 1 1)$ pole figures in Fig. 2(a₂), the as-cast alloy has a nearly random texture. After 1 pass of ECAP (Fig. 2(b₂)), the original as-cast texture has been significantly changed. A strong shear-type texture with a maximum intensity of ~ 5.9 mr (multiply random) is formed, showing six almost equal-spaced peaks. The nearly monoclinic symmetry can be identified, which refers to the invariance about a 180° rotation around the TD axis. Furthermore, the $\langle 1 1 0 \rangle$ directions tend to align with the shear direction (45° to ED) and the $\{1 1 1\}$ planes tend to be in line with the shear plane (with their normal directions perpendicular to the shear plane). It indicates that both the $\{1 1 1\}_\theta$ -fiber and $\{1 1 0\}_\theta$ -fiber [15, 44] have formed. This is in good agreement with both the simulation [25] and experimental results [28] in other works, where a clear shear-type texture can be identified regardless of initial textures.

After 3 passes of ECAP (Fig. 2(c₂)), compared to the 1P sample, the texture components become more concentrated with the maximum intensity increased to ~ 9.1 mr. However, as can be observed from the $(1 1 0)$ pole figure, some pole peaks have faded. The texture orientation components at the edge of the great circle in the $(1 1 1)$ pole figure have rotated a little in the clockwise sense around the TD axis. The maximum intensity value of both the $\{1 1 1\}_\theta$ -fiber and $\{1 1 0\}_\theta$ -fiber components increases.

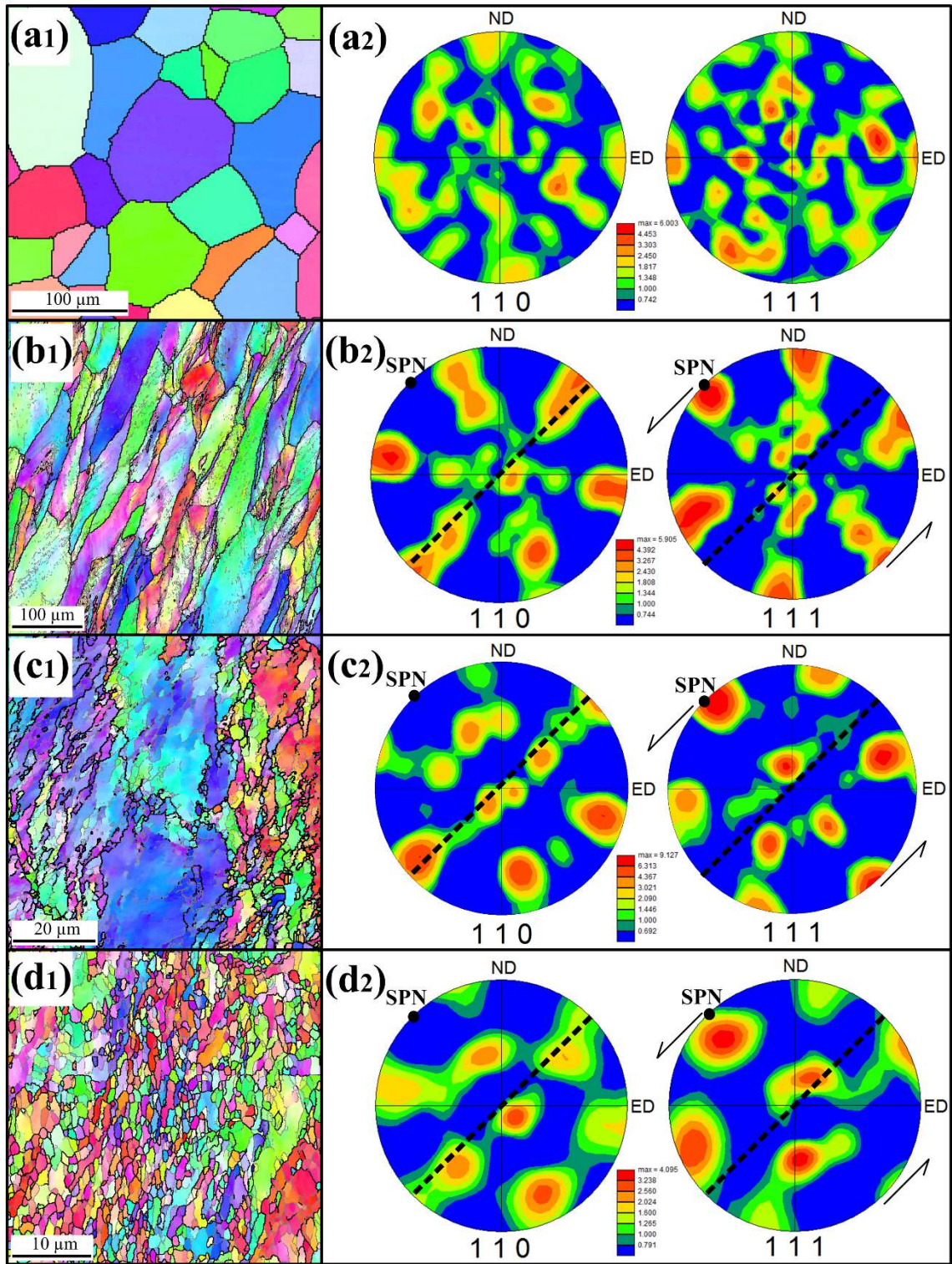


Fig. 2. Microstructures and pole figures (in the ND-ED projection) of ECAP processed Al-8Zn samples via route Bc. (a₁) and (a₂) Before ECAP, (b₁) and (b₂) 1P, (c₁) and (c₂) 3P, and (d₁) and (d₂) 5P. In IPF maps, grey and black lines depict boundaries with misorientation angles of $5^\circ \leq \theta < 15^\circ$ and $15^\circ \leq \theta < 180^\circ$, respectively. In pole figures, the shear plane is indicated by the dashed line while SPN represents the shear plane normal.

With further increasing the strain to $\varepsilon = 5$ (5 ECAP passes), the monoclinic symmetry cannot be well identified. Both of the $\{1\ 1\ 0\}_\theta$ -fiber and $\{1\ 1\ 1\}_\theta$ -fiber components have deviated away from the shear direction and shear plane, respectively. Besides, the maximum intensity of both the $\{1\ 1\ 0\}_\theta$ -fiber and $\{1\ 1\ 1\}_\theta$ -fiber components shows a decreasing trend. As indicated in Fig. 1(c), route Bc is a cyclic process of 4 ECAP passes. The shear plane of the 5th pass is the same as that of the 1st pass, but the ECAP texture of the 5P sample is different from that of the 1st pass. The main differences between the 1st and 5th pass is the “initial texture” and the extent of grain refinement as a result of CDRX. However, it has been demonstrated that the initial texture only influences the texture intensity while the ECAP texture orientations are much less affected [17, 45]. Thus, the CDRX process is the main reason for the loss of monoclinic symmetry and deviation from ideal positions.

Fig. 3(a) shows the IPF map of the 3P sample, where coarse and fine grains can be clearly seen. For the fine grains, when considered as a whole aggregate, they show characteristics of the ideal ECAP texture, as confirmed by the pole figures of the region 1 and region 2 in Fig. 3(b) and (c), respectively. However, when consider the fine grains separately, for some of them, such as the fine grains G1 and G2 highlighted in Fig. 3(a), neither the $\langle 1\ 1\ 0 \rangle$ directions are in line with the shear direction, nor the $\{1\ 1\ 1\}$ planes are parallel to the shear plane. It means that orientations of these fine grains greatly deviate from the main ECAP texture components as shown in Fig. 2(c₂). This can be related to the additional rotation of these fine grains due to CDRX.

Fig. 3(f) and (g) show $(1\ 1\ 0)$ and $(1\ 1\ 1)$ pole figures of the coarse grains G3 and G4. As can be clearly identified, for the coarse grain G3, one of the $\langle 1\ 1\ 0 \rangle$ directions parallels to the shear direction. However, as indicated in Fig. 3(g), the coarse grain G4 is different from grain G1. One of its $\langle 1\ 1\ 0 \rangle$ directions is in line with the shear direction while one of the $\{1\ 1\ 1\}$ planes parallels to the shear plane. It confirms that the coarse grain G3 gives rise to the $\{1\ 1\ 0\}_\theta$ -fiber components, whereas the coarse grain G4 leads to both the $\{1\ 1\ 0\}_\theta$ -fiber and $\{1\ 1\ 1\}_\theta$ -fiber components. These two examples of coarse grains reveal that although the coarse grains are less deformed, they have rotated to orientations that contribute to the main texture components shown in Fig. 2(c₂).

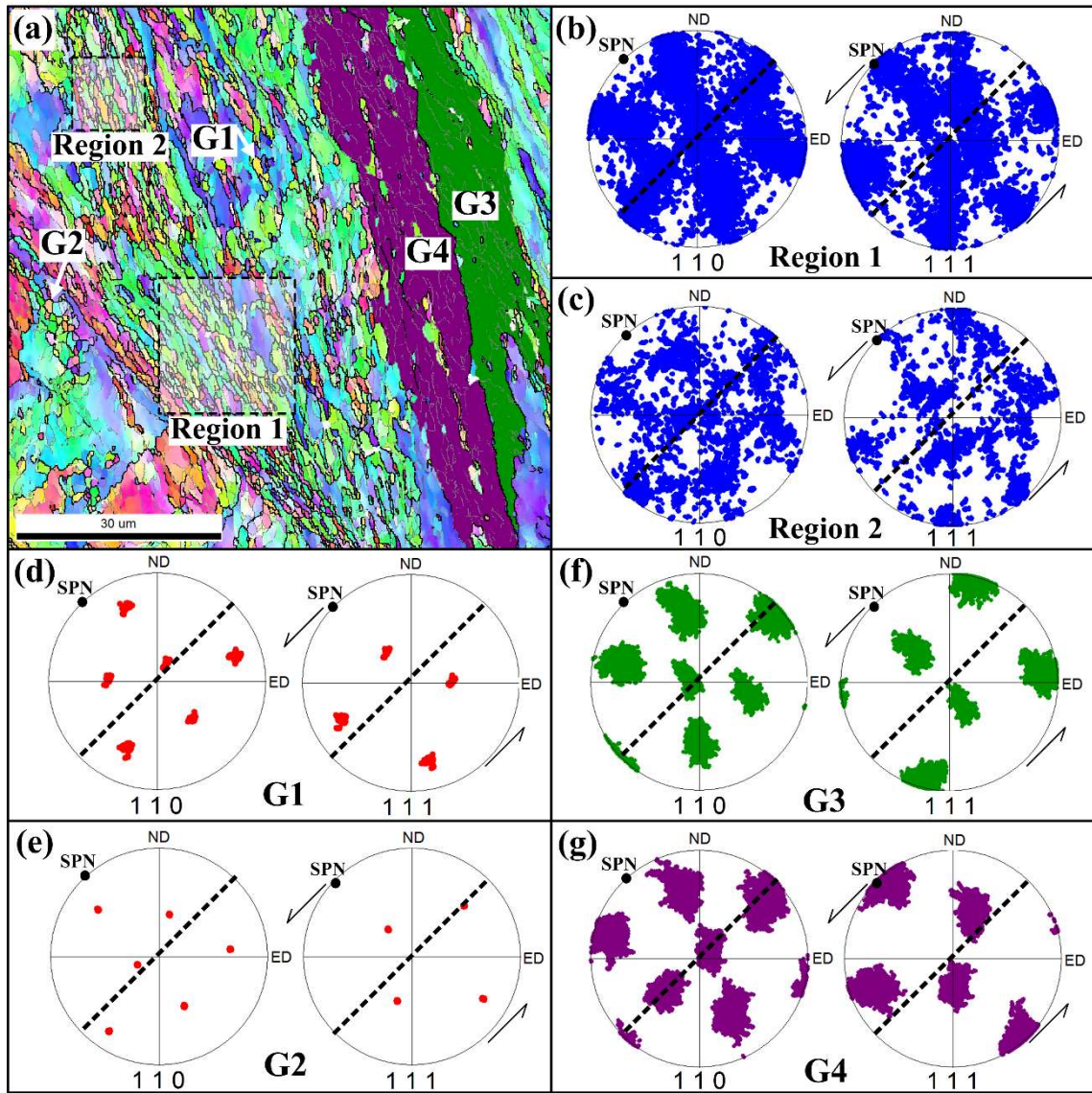


Fig. 3. IPF map of the 3P Al-8Zn sample and corresponding pole figures (PFs) of highlighted grains and regions. (a) IPF map, (b) PFs of Region 1, and (c) PFs of Region 2, (d) PFs of the fine grain G1, (e) PFs of the fine grain G2, (f) PFs of the coarse grain G3, and (g) PFs of the coarse grain G4.

In addition to pole figures, ODF plots have also been made to demonstrate more clearly the character of ECAP texture. The main ideal ECAP texture components are denoted as A_θ , A_θ^* , B_θ , and C_θ [21], which are given in the form of Euler angles (only in the $\varphi_2 = 0^\circ$ and 45° sections) in Table 1. As shown in Fig. 4(a), ODF plots separate the components that partially overlap in pole figures (e.g. A_θ , \bar{A}_θ and $A_{1\theta}^*$), allowing for a more unambiguous comparison of the individual components and fibers. Studies on ECAP texture of FCC materials have introduced the so-called f1, f2 and f3 fibers

[12, 21]. The f1 fiber is composed of the $A_{10}^* - A_{\theta} - A_{20}^* \{1\ 1\ 1\}_{\theta}$ partial fiber [21]. The f2 fiber includes the $C_{\theta} - \bar{B}_{\theta} - \bar{A}_{\theta}$ orientations along $\langle 1\ 1\ 0 \rangle_{\theta}$ and the $\bar{A}_{\theta} - A_{10}^*$ orientations along $\{1\ 1\ 1\}_{\theta}$, which meet at the \bar{A}_{θ} position [21]. The f3 fiber consists of the $C_{\theta} - B_{\theta} - A_{\theta} - A_{20}^*$ orientations [21].

Table 1. Ideal orientations (given in the $\varphi_2 = 0^\circ$ and 45° sections only) and fibers of interest for FCC materials in a single pass of ECAP using a $\Phi = 90^\circ$ die [21].

Component Notation	Euler angles ($^\circ$)			Fibers that the component belongs to
	φ_1	Φ	φ_2	
A_{10}^*	80.26/260.26	45	0	$\{1\ 1\ 1\}_{\theta}$
	170.26/350.26	90	45	
A_{20}^*	9.74/189.74	45	0	$\{1\ 1\ 1\}_{\theta}$
	99.74/279.74	90	45	
A_{θ}	45	35.26	45	$\{1\ 1\ 1\}_{\theta}, \langle 1\ 1\ 0 \rangle_{\theta}$
\bar{A}_{θ}	225	35.26	45	$\{1\ 1\ 1\}_{\theta}, \langle 1\ 1\ 0 \rangle_{\theta}$
B_{θ}	45/165/285	54.74	45	$\langle 1\ 1\ 0 \rangle_{\theta}$
\bar{B}_{θ}	105/225/345	54.74	45	$\langle 1\ 1\ 0 \rangle_{\theta}$
C_{θ}	135/315	45	0	$\langle 1\ 1\ 0 \rangle_{\theta}$
	45/225	90	45	

To facilitate comparisons of textures developed after different passes, we plotted the $\varphi_2 = 0^\circ, 15^\circ, 30^\circ, 45^\circ, 60^\circ, 75^\circ, 90^\circ$ ODF sections, with $\Phi = 0-90^\circ$ and $\varphi_1 = 0-180^\circ$. In Fig. 4(b)-(d), the dotted lines represent the ideal orientations constituting the f1-f3 fibers as mentioned above. After 1 pass (Fig. 4(b)), the dotted lines can be observed to trace most of the highly populated orientations although there are some slight deviations. The near-monoclinic symmetry of the 1 pass ECAP texture can be observed, since the orientation distributions are approximately symmetric in the $\varphi_1 = 0-180^\circ$ and $\varphi_1 = 180-360^\circ$ intervals. Specifically, as can be seen from the $\varphi_2 = 0^\circ$ and the $\varphi_2 = 45^\circ$ sections, the A_{10}^* component is strong and the $B_{\theta}/\bar{B}_{\theta}$ components are moderate, while the A_{20}^* component is weak. This is similar to the results in the work [26], even though the initial texture in the work [26] exhibits strong $(1\ 0\ 0)$ and $(1\ 1\ 1)$ fibers. It further indicates that the initial texture plays a very limited role on the ECAP texture.

After 3 passes, the maximum intensity has increased from ~ 18.1 to ~ 36.9 mr. It is clear that the near-monoclinic symmetry is not maintained, such as the large difference in orientation densities

between A_θ and \bar{A}_θ , and B_θ and \bar{B}_θ . The loss of near-monoclinic symmetry is also reflected in the different orientation distributions along fibers in the $\varphi_1 = 0\text{-}180^\circ$ and $\varphi_1 = 180\text{-}360^\circ$ intervals. Nevertheless, main texture components can still be depicted along f1-f3 fibers, but the fibers appear to be much less complete compared to those of the 1P sample, such as the lack of orientations near C_θ .

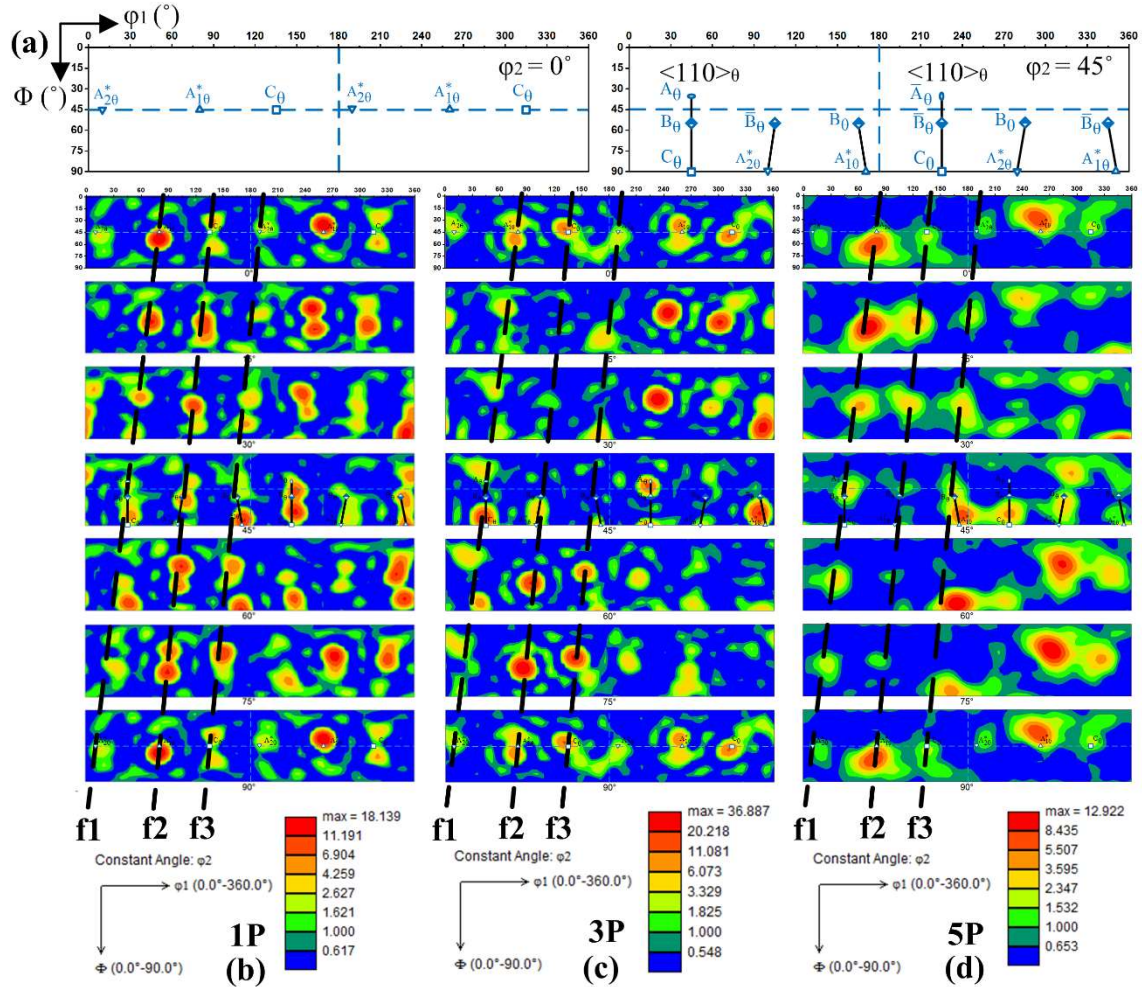


Fig. 4. (a) The $\varphi_2 = 0^\circ$ and 45° ODF sections [23], showing the main ideal orientations of FCC materials deformed by a 90° ECAP die, and ODF sections ($\varphi_2 = \text{constant}$) of textures measured after (b) 1P, (c) 3P and (d) 5P. The dotted lines represent the ideal orientations constituting the f1, f2 and f3 fibers.

With increasing the number of ECAP passes to 5, the maximum intensity decreases compared to those of the 1P and 3P samples. It can be observed that the main texture orientations of the f1 and f3 fibers become less concentrated to some extent. Moreover, the $A_{2\theta}^*$ component is still almost absent. As indicated in the $\varphi_2 = 45^\circ$ section, compared with the 1P sample, the $\langle 110 \rangle_\theta$ -fiber becomes less completed, which is consistent with the PF results in Fig. 2(d₂). Considering the 4-pass cyclic

deformation in route Bc, it is interesting to compare textures of the 1P and 5P samples. The fading of the f1, f2 and f3 fibers can be clearly seen, especially the f2 fiber in the $\varphi_1 = 0-180^\circ$ interval, which further indicates that the CDRX process can weak the ECAP texture.

3.2. Microstructural evolution during annealing

Fig. 5 shows EBSD IPF and boundary maps of the 5P sample annealed at 200 °C for different times. Compared to the 5P sample (Fig. 2(d₁)), after annealing for 2 h, limited grain growth can be observed. It indicates that recovery is the main process that takes place in the structure, i.e., thermally activated annihilation and rearrangement of dislocations. As demonstrated in our previous work [42], in the 5P sample, dynamic recovery and recrystallization during ECAP deformation have fulfilled to such an extent that most dislocations are already in the form of well-developed (sub)grain structures. Therefore, although the number of dislocations in the grain interiors decreases, few new (sub)grains can form.

With further increasing the annealing time to 8 h (Fig. 5(b)), typical discontinuous recrystallization still cannot be observed, i.e., “recrystallized” and “unrecrystallized” regions cannot be well distinguished. The as-deformed (5P) alloys have transform into a reasonably homogeneous microstructure, which means that “extended recovery” has occurred. It can be seen that the number density of ultrafine grains (with grain sizes less than 1 μm) shows a decreasing trend and the average grain size becomes larger ($\sim 1.3 \mu\text{m}$), which indicates coarsening of the grain structure. After annealing for 96 h (Fig. 5(c)), the average grain size has further increased to $\sim 2.2 \mu\text{m}$. Some dislocation-free grains with dimensions larger than 10 μm appear, which has consumed the smaller ones as a result of their faster growing rate.

Fig. 5(d) presents the large-scale microstructure of the 5P sample after annealing for 240 h. It can be seen that on a large scale, a significantly heterogeneous microstructure has formed. Some coarsened grains separated by high angle boundaries appear to be with an elongated shape along the ED axis. Some grains are much finer, showing a large fraction of low angle boundaries. This kind of heterogenous microstructure is a result of inheriting the microstructure of the 5P sample. As shown in Fig. 2(d₁), in the 5P sample, some coarse grains bounded by high angle boundaries exist. Compared to

the well dynamically recrystallized ultrafine grains, these coarse grains are with a higher dislocation density. Therefore, coarse grains recover faster during annealing at 200 °C, followed by growing and consuming the less recovered region.

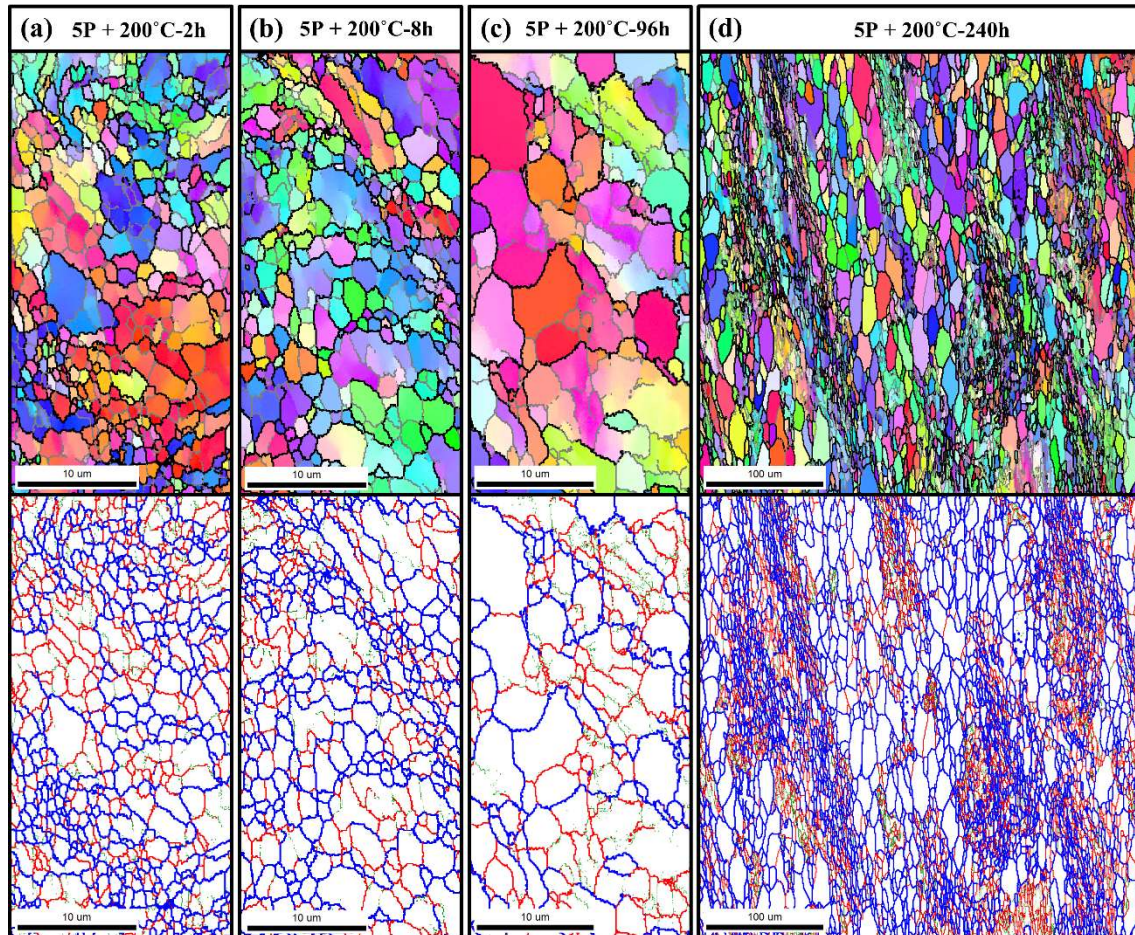


Fig. 5. EBSD IPF maps and boundary maps of the Al-8Zn alloy annealed at 200 °C for different times. (a) 5P + 2 h, (b) 5P + 8 h, (c) 5P + 96 h and (d) 5P + 240 h. In IPF maps, grey lines and black lines depict boundaries with misorientation angles of $5^\circ \leq \theta < 15^\circ$ and $15^\circ \leq \theta < 180^\circ$, respectively. In boundary maps, green, red and blue lines depict boundaries with misorientation angles of $2^\circ \leq \theta < 5^\circ$, $5^\circ \leq \theta < 15^\circ$ and $15^\circ \leq \theta < 180^\circ$, respectively.

In order to study the microstructural evolution during static recrystallization, annealing was carried out at a higher temperature of 350 °C. Quasi-in-situ EBSD was conducted on the 5P sample annealed at 350 °C, which means that the measurements were performed on the same area as close as possible. Fig. 6 shows the IPF and kernel average misorientation (KAM) maps of the 5P sample annealed at 350 °C for different times. After annealing at 350 °C for 2 min (Fig. 6(a)), two types of regions with clearly different microstructures can be classified. Most of the material has recrystallized,

leaving few areas with fine grains surrounded by low angle boundaries and contain a relatively higher dislocation density, such as the areas highlighted by the white circles. The recrystallized areas are with much coarsened equiaxed grains, which appear to be mainly delineated by high angle boundaries. As highlighted in the IPF map in Fig. 6(a), the grains G1 and G5 are just recrystallized, while the grains G2-G4 and G6 have grown to a larger extent.

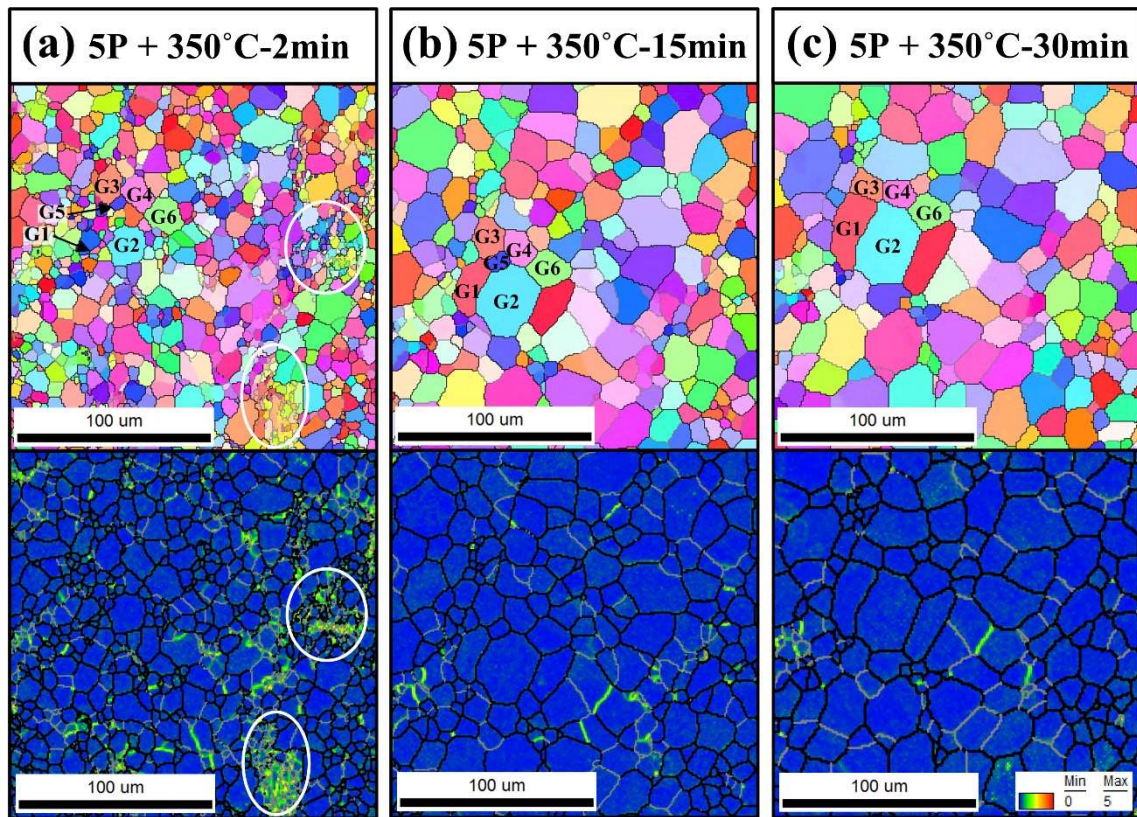


Fig. 6. EBSD IPF maps and Kernel average misorientation maps of the Al-8Zn alloy annealed at 350 °C. (a) 5P + 2 min, (b) 5P + 15 min and (c) 5P + 30 min. Grey lines and black lines depict boundaries with misorientation angles of $5^\circ \leq \theta < 15^\circ$ and $15^\circ \leq \theta < 180^\circ$, respectively.

With increasing the annealing time to 15 min, the microstructure is fully recrystallized. It can be seen that the grain G1 has grown greatly, while the grains G3-G6 are with a slower growing rate. The grains between grains G1, G2 and G5 have completely consumed by the grains G1 and G2. With further increasing the annealing time to 30 min, the grain growth rate becomes slower compared to that within 15 min. The grain shape is close to equiaxed, with an average grain size of $\sim 12.4 \mu\text{m}$. By comparing the IPF maps in Fig. 6(b) and (c), it can be seen that the grain G5 has been consumed completely by the grains G1 and G2, which indicates that compared to the grains G3-G5, the grains G1 and G2 are with a priority to grow.

3.3. Influence of annealing on ECAP texture

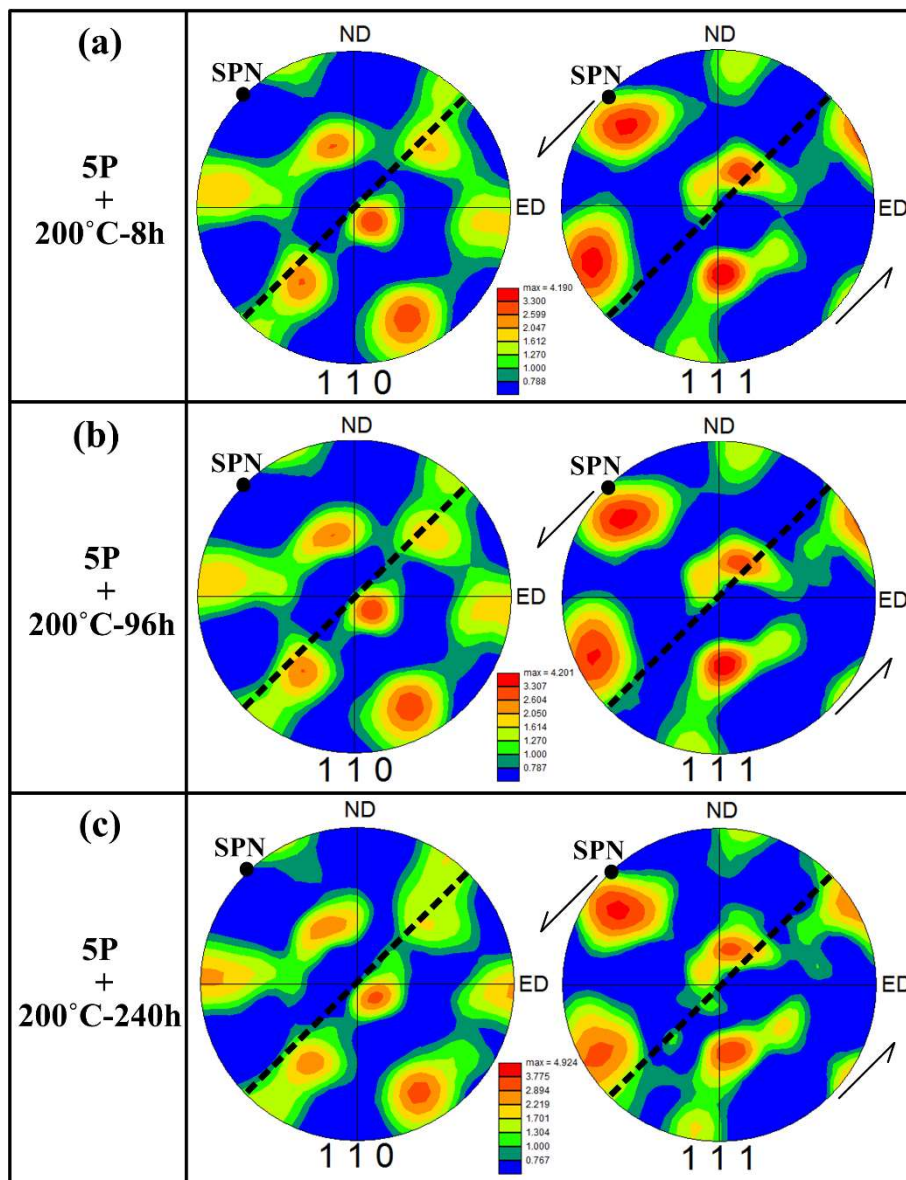


Fig. 7. (1 1 0) and (1 1 1) pole figures of 5P Al-8Zn alloy annealed at 200 °C. (a) 8 h, (b) 96 h and (c) 240 h. The dotted lines in pole figures indicate the ideal shear plane and SPN is the shear plane normal.

The effect of annealing at 200 °C on ECAP texture is illustrated by pole figures in Fig. 7. After annealing at 200 °C for 8 h, the texture remains quite similar to that of the 5P sample (Fig. 2(d₂)). It means that this annealing condition does not change the texture very much, demonstrating that extended recovery is not radical enough to eliminate original ECAP fibers. This is because no nucleation of new crystals with orientations totally different from their parent grains. With increasing the annealing time to 96 h at 200 °C, despite grain growth happens, the textures are still close to those

of the 5P and 5P+8h samples. After annealing at 200 °C for a very long time of 240 h, orientations of the main ECAP texture components are still almost identical to that of the 5P sample, with limited increase of the maximum intensity. It indicates that grains contribute to the main ECAP texture components grow at a similar rate.

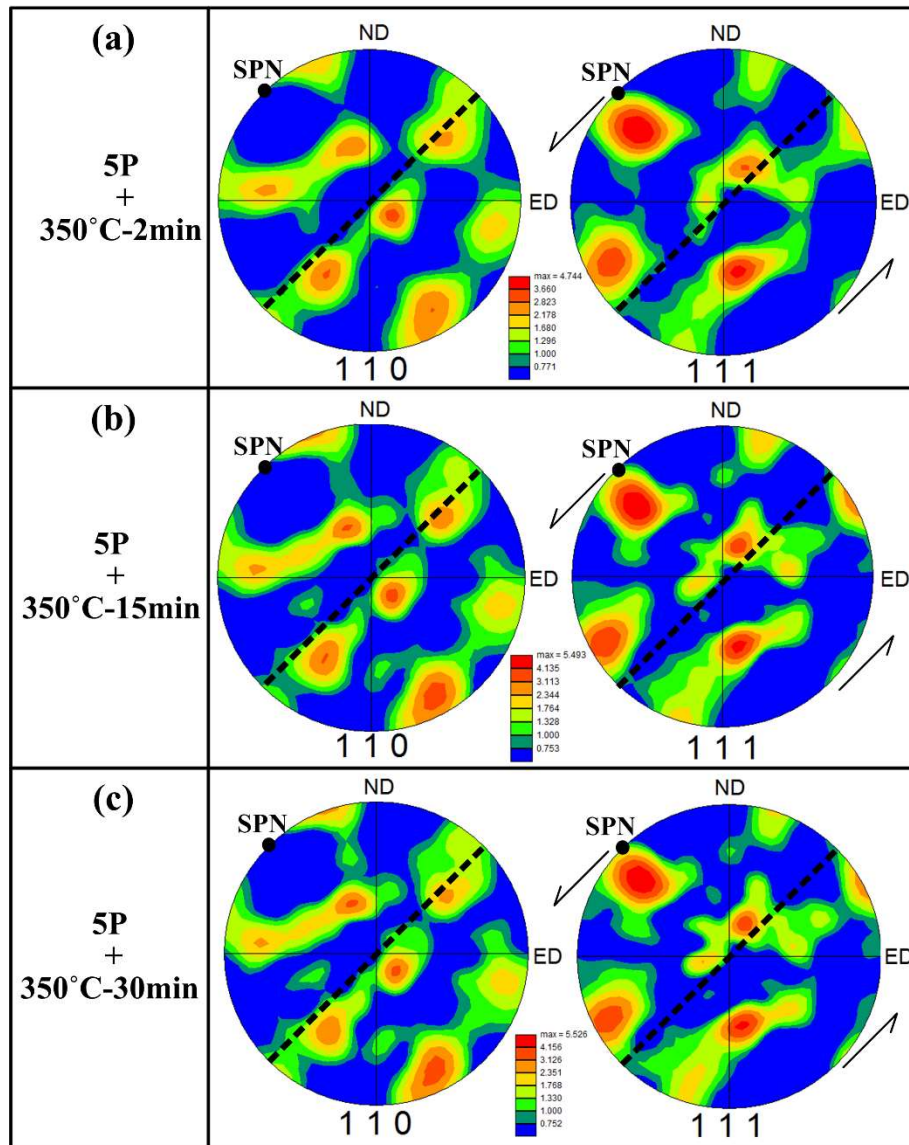


Fig. 8. (1 1 0) and (1 1 1) pole figures of 5P Al-8Zn alloy annealed at 350 °C. (a) 2 min, (b) 15 min and (c) 30 min. The dotted lines in pole figures indicate the ideal shear plane and SPN is the shear plane normal.

As can be observed from Fig. 8, after annealing at a higher temperature of 350 °C, orientations of the main ECAP texture components are quite similar to that of the 5P and 5P samples annealed at 200 °C, but with higher maximum intensities. Therefore, fully recrystallization and subsequent grain growth cannot modify the as-deformed (5P) ECAP texture. It reveals that the formation of new grains

during static recrystallization cannot give rise to new orientations developed against those of the as-deformed grains. Also, there seems to be limited preferential grain growth of the recrystallized grains with special grain orientations. This has been further clarified by pole figures of partitioned grains with different grain sizes in 5P + 2 min sample. As can be seen from Fig. 9, the pole figures of grains with the grain size $\leq 2 \mu\text{m}$, $2\text{-}10 \mu\text{m}$, and $\geq 10 \mu\text{m}$ show similar characteristics to that of the 5P + 2 min sample (Fig. 8(a)).

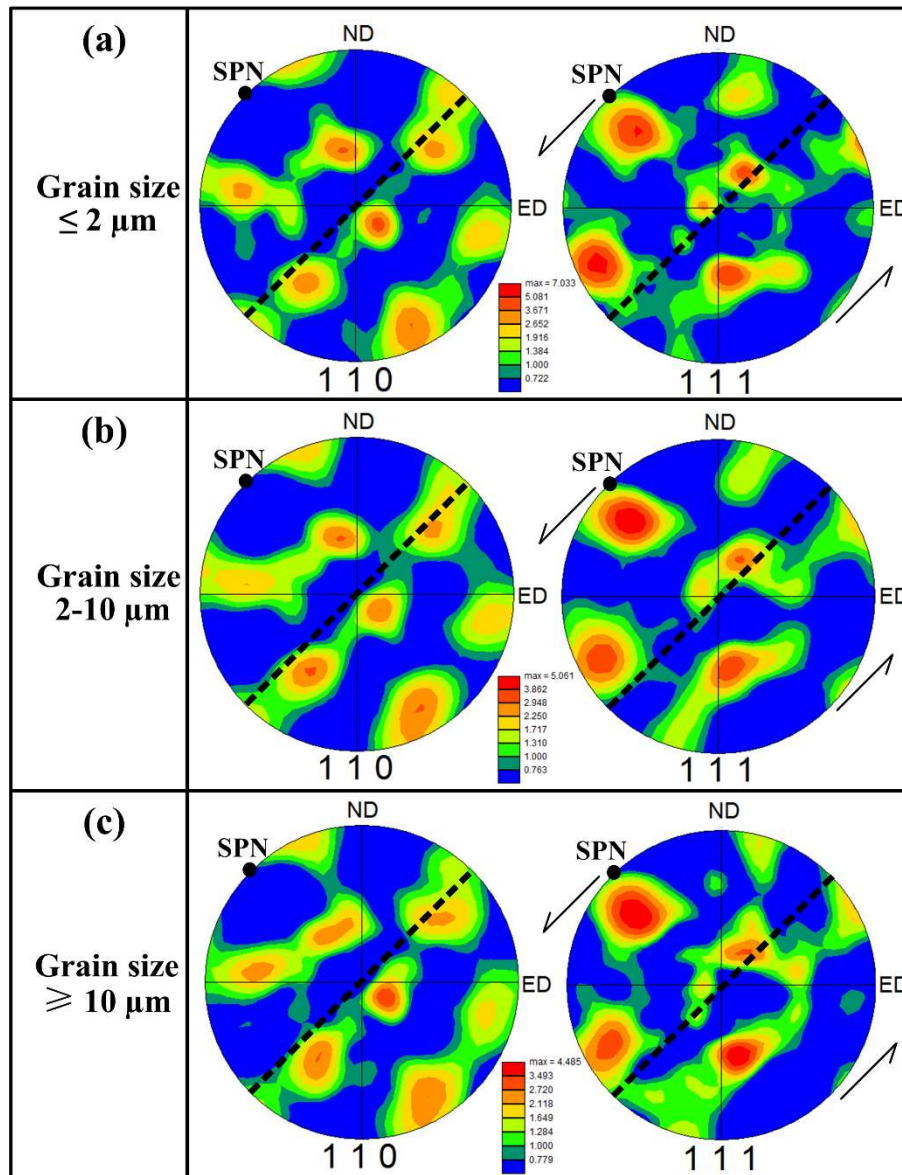


Fig. 9. (1 1 0) and (1 1 1) pole figures of grains with different sizes in the 5P + 2 min sample annealed at 350 °C. (a) Grain size $\leq 2 \mu\text{m}$, (b) $2 \mu\text{m} < \text{grain size} < 10 \mu\text{m}$ and (c) grain size $\geq 10 \mu\text{m}$. The dotted lines in pole figures indicate the ideal shear plane and SPN is the shear plane normal.

The similarity between texture of the 5P sample and the annealed 5P sample can be also confirmed by the selected $\varphi_2 = \text{constant}$ ODF sections in Fig. 10. In comparison to the 5P sample, positions of the main texture components in ODF plots becomes more spread, which is more obvious when annealing at 350 °C. In addition, little increase in the maximum intensities of the 5P samples annealed at 200 °C can be observed, while annealing at 350 °C results in larger maximum intensities. Furthermore, recrystallization (annealing at 350 °C) leads to decreases in the maximum intensity of A_{10}^* and C_0 orientations.

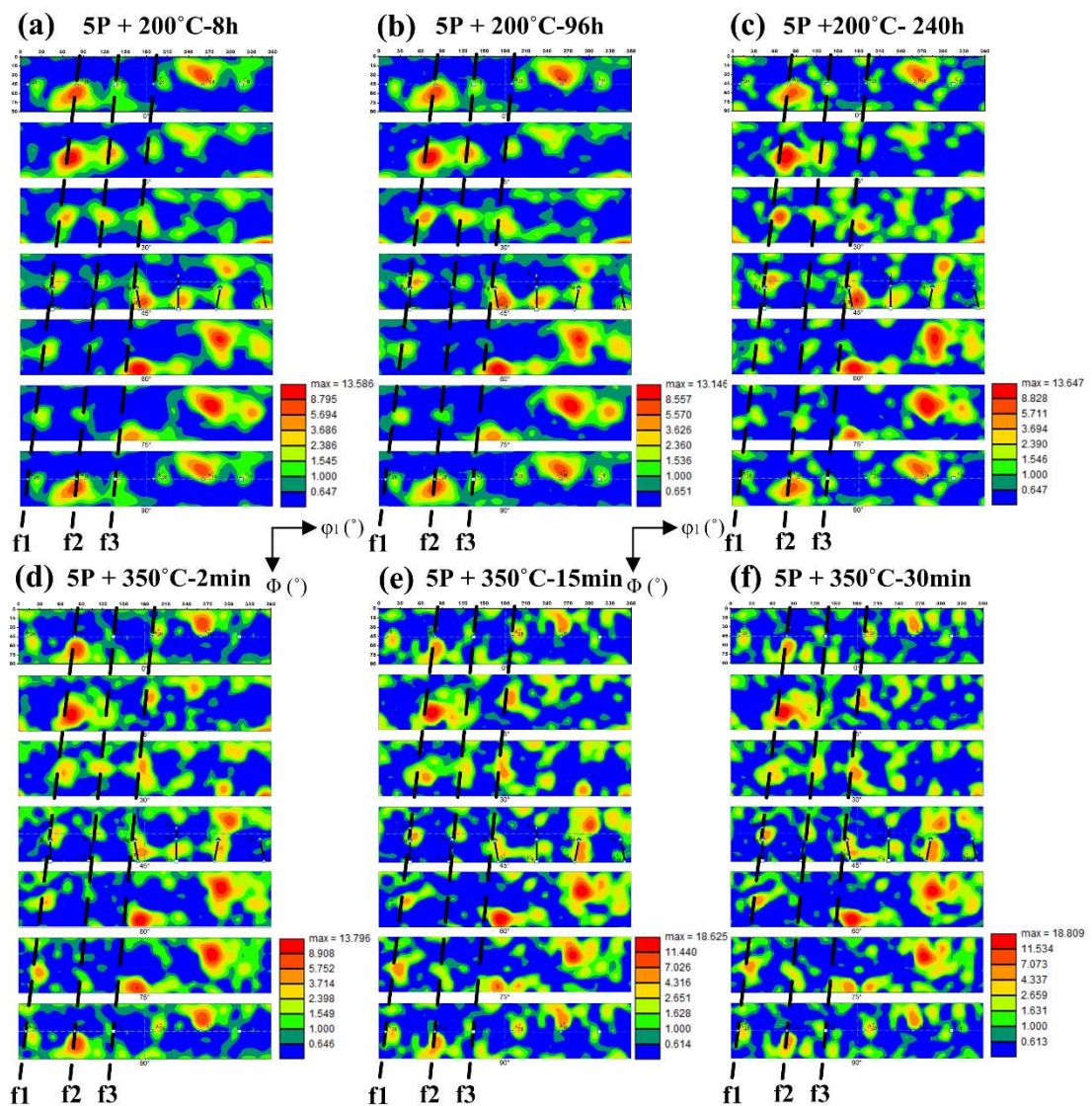


Fig. 10. ODF sections ($\varphi_2 = \text{constant}$) of the 5P sample measured after annealing at 200 °C and 350 °C. (a) 200 °C-8 h, (b) 200 °C-96 h, (c) 200 °C-240 h, (d) 350 °C-2 min, (e) 350 °C-15 min and 350 °C-30 min. The dotted lines represent the ideal orientations constituting the f1, f2 and f3 fibers.

In order to ascertain the evolution of the f1-f3 fibers, their intensities are represented by the number fraction of selected orientations (with a 5° spread) defined as highly populated orientations constituting the f1, f2 and f3 fibers. It can be observed from Fig. 10 that the further deformation after 3 passes of ECAP does not change the intensity of all the three fibers very much, while after 5 passes of ECAP, the intensity decreases sharply. Overall, static recovery and recrystallization during isothermal annealing lead to limited changes (1-3%) in the fraction of f1-f3 fibers, which is consistent with the results as revealed by pole figures (Fig. 7 and 8). Also, grain growth exerts little influence on the ECAP texture, such as annealing at 200 °C for 240 h and at 350 °C for 30 min. Among all the three fibers, fiber 3 shows an increasing trend after annealing at 200 °C for 240 h and at 350 °C for 30 min. The evolution of the total fraction of f1-f3 fibers implies the weakening of texture during ECAP, while static recovery and recrystallization during post-ECAP isothermal annealing have a limited influence on the ECAP texture.

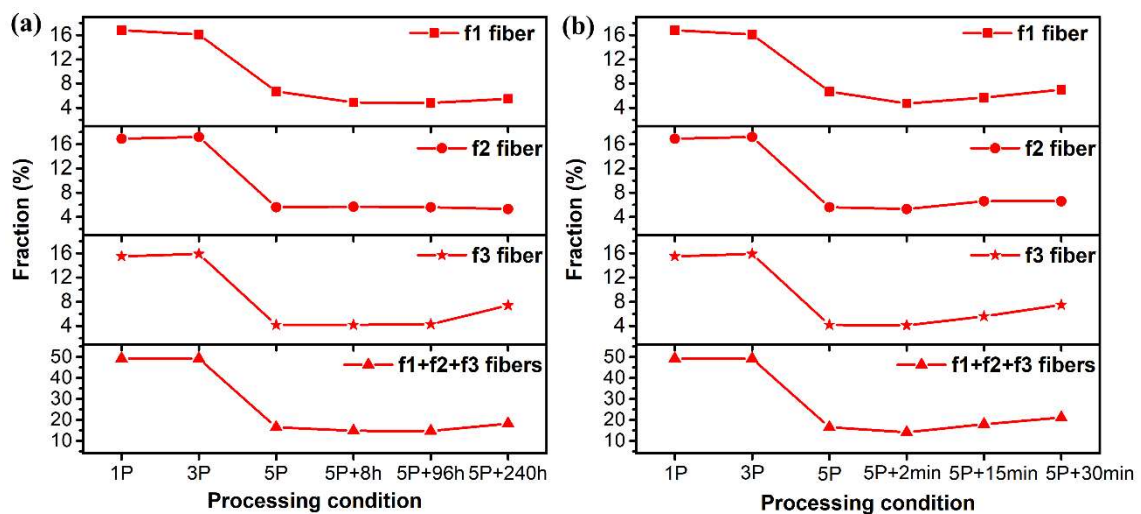


Fig. 11. Fraction evolution of the three main texture fibers (f1-f3) as well as the total of f1-f3 fibers with a spread angle of 5°. (a) Annealing at 200 °C, and (b) annealing at 350 °C. For comparison, the fractions of the three main texture fibers (f1-f3) of the as-ECAPed samples have also been given in (a) and (b).

4. Conclusions

The Al-8Zn alloy was subjected to ECAP via route Bc and post-ECAP isothermal annealing at 200 °C and 350 °C. A complete study on the microstructural and texture evolution as well as their

interaction was carried out by EBSD. This study provides an insight into the influence of post-ECAP annealing on texture, in terms of recovery and fully static recrystallization. The following main conclusions can be drawn.

(1) After 1 pass of ECAP, the ECAP texture is similar to the ideal shear texture. During deformation, even though the coarse grains are less deformed, they have rotated towards the ideal ECAP texture orientations.

(2) With increasing the number of ECAP passes to 5, the main texture components can still be depicted by fibers f1-f3. However, fading of the f1, f2 and f3 fibers occurs, resulting in less completed f1-f3 fibers.

(3) The quantified study of texture evolution by calculating the fraction of the main texture fibers with a spread angle of 5° , ascertained the weakening of ECAP texture after 5 passes via route Bc due to CDRX.

(4) Only recovery occurs upon annealing at 200°C for 2 h, while the coarsening of UFG grains are depressed. The grain structure is thermally stable up to 8 h at 200°C with slight grain coarsening.

(5) The ECAP texture of the 5P sample shows a stability when annealing at 200°C up to 240 h, keeping the main orientations and intensity almost unchanged. The reason is that grains contribute to the main ECAP texture components grow at a similar rate.

(6) After annealing at a higher temperature of 350°C , recrystallization occurs. However, orientations of the main ECAP texture components are quite similar to that of the 5P and 5P samples annealed at 200°C , but with higher maximum intensities. Also, there seems to be limited preferential grain growth of the recrystallized grains. It indicates that fully recrystallization and subsequent grain growth can hardly modify the as-deformed (5P) ECAP texture.

Acknowledgements

The authors would like to acknowledge the financial support from Research Council of Norway, under the FRINATEK project 'BENTMAT' (Project number 222173). The authors also appreciate Mr. Pål C. Skaret for his assistance during the ECAP experiment.

References

- [1] M.H. Shaeri, M. Shaeri, M. Ebrahimi, M.T. Salehi, S.H. Seyyedein, Effect of ECAP temperature on microstructure and mechanical properties of Al–Zn–Mg–Cu alloy, *Progress in Natural Science: Materials International* 26(2) (2016) 182-191.
- [2] M.A. Afifi, Y.C. Wang, P.H.R. Pereira, Y. Huang, Y. Wang, X. Cheng, S. Li, T.G. Langdon, Mechanical properties of an Al-Zn-Mg alloy processed by ECAP and heat treatments, *Journal of Alloys and Compounds* 769 (2018) 631-639.
- [3] A.F. Abd El-Rehim, M.M. El-Sayed, M.R. Nagy, M.A. El-Hafez, Influence of quenching conditions on the mechanical and structural properties of Al–30wt% Zn alloy, *Materials Science and Engineering: A* 602 (2014) 105-109.
- [4] S. Popović, B. Gržeta, Precipitation and Dissolution phenomena in Al-Zn alloys, *Croatica Chemica Acta* 72(2-3) (1999) 621-643.
- [5] T. Savaşkan, A.P. Hekimoğlu, G. Pürçek, Effect of copper content on the mechanical and sliding wear properties of monotectoid-based zinc-aluminium-copper alloys, *Tribology International* 37(1) (2004) 45-50.
- [6] H.L. Jia, R. Bjørge, K. Marthinsen, Y.J. Li, The deformation and work hardening behaviour of a SPD processed Al-5Cu alloy, *Journal of Alloys and Compounds* 697 (2017) 239-248.
- [7] H.L. Jia, R. Bjørge, L.F. Cao, H. Song, K. Marthinsen, Y.J. Li, Quantifying the grain boundary segregation strengthening induced by post-ECAP aging in an Al-5Cu alloy, *Acta Materialia* 155 (2018) 199-213.
- [8] H.L. Jia, S.B. Jin, Y.J. Li, Formation of $\Sigma\{110\}$ incoherent twin boundaries through geometrically necessary boundaries in an Al-8Zn alloy subjected to one pass of equal channel angular pressing, *Journal of Alloys and Compounds* 762 (2018) 190-195.
- [9] H.L. Jia, K. Marthinsen, Y.J. Li, Al-5Cu Alloy Processed by Equal-Channel Angular Pressing, *Materials Science Forum*, Trans Tech Publ, 2017, pp. 843-848.
- [10] R.Z. Valiev, T.G. Langdon, Principles of equal-channel angular pressing as a processing tool for grain refinement, *Progress in Materials Science* 51(7) (2006) 881-981.
- [11] H.L. Jia, K. Marthinsen, Y.J. Li, Effect of soft Bi particles on grain refinement during severe plastic deformation, *Transactions of Nonferrous Metals Society of China* 27(5) (2017) 971-976.
- [12] S. Li, I.J. Beyerlein, D.J. Alexander, S.C. Vogel, Texture evolution during equal channel angular extrusion: Effect of initial texture from experiment and simulation, *Scripta Materialia* 52(11) (2005) 1099-1104.
- [13] W. Skrotzki, N. Scheerbaum, C.G. Oertel, H.G. Brokmeier, S. Suwas, L.S. Tóth, Recrystallization of high-purity aluminium during equal channel angular pressing, *Acta Materialia* 55(7) (2007) 2211-2218.
- [14] A. Gholinia, P. Bate, P.B. Prangnell, Modelling texture development during equal channel angular extrusion of aluminium, *Acta Materialia* 50(8) (2002) 2121-2136.
- [15] S.D. Terhune, D.L. Swisher, K. Oh-Ishi, Z. Horita, T.G. Langdon, T.R. McNelley, An investigation of microstructure and grain-boundary evolution during ECA pressing of pure aluminum, *Metallurgical and Materials Transactions A* 33(7) (2002) 2173-2184.
- [16] W.Q. Cao, A. Godfrey, Q. Liu, EBSD investigation of microstructure and texture evolution during equal channel angular pressing of aluminium, *Materials Science and Engineering: A* 361(1–2) (2003) 9-14.
- [17] S. Ferrasse, V.M. Segal, S.R. Kalidindi, F. Alford, Texture evolution during equal channel angular extrusion: Part I. Effect of route, number of passes and initial texture, *Materials Science and Engineering: A* 368(1) (2004) 28-40.
- [18] S. Ferrasse, V.M. Segal, F. Alford, Texture evolution during equal channel angular extrusion (ECAE): Part II. An effect of post-deformation annealing, *Materials Science and Engineering: A* 372(1) (2004) 235-244.
- [19] A.P. Zhilyaev, D.L. Swisher, K. Oh-ishi, T.G. Langdon, T.R. McNelley, Microtexture and microstructure evolution during processing of pure aluminum by repetitive ECAP, *Materials Science and Engineering: A* 429(1) (2006) 137-148.

- [20] A.A. Salem, T.G. Langdon, T.R. McNelley, S.R. Kalidindi, S.L. Semiatin, Strain-path effects on the evolution of microstructure and texture during the severe-plastic deformation of aluminum, *Metallurgical and Materials Transactions A* 37(9) (2006) 2879-2891.
- [21] S. Li, I.J. Beyerlein, D.J. Alexander, S.C. Vogel, Texture evolution during multi-pass equal channel angular extrusion of copper: Neutron diffraction characterization and polycrystal modeling, *Acta Materialia* 53(7) (2005) 2111-2125.
- [22] X. Molodova, G. Gottstein, M. Winning, R.J. Hellmig, Thermal stability of ECAP processed pure copper, *Materials Science and Engineering: A* 460-461 (2007) 204-213.
- [23] S. Li, I.J. Beyerlein, M.A.M. Bourke, Texture formation during equal channel angular extrusion of fcc and bcc materials: comparison with simple shear, *Materials Science and Engineering: A* 394(1) (2005) 66-77.
- [24] L.S. Tóth, R. Arruffat Massion, L. Germain, S.C. Baik, S. Suwas, Analysis of texture evolution in equal channel angular extrusion of copper using a new flow field, *Acta Materialia* 52(7) (2004) 1885-1898.
- [25] S. Li, I.J. Beyerlein, C.T. Necker, D.J. Alexander, M. Bourke, Heterogeneity of deformation texture in equal channel angular extrusion of copper, *Acta Materialia* 52(16) (2004) 4859-4875.
- [26] M.H. Shaeri, M.T. Salehi, S.H. Seyyedein, M.R. Abutalebi, J.K. Park, Characterization of microstructure and deformation texture during equal channel Angular pressing of Al-Zn-Mg-Cu alloy, *Journal of Alloys and Compounds* 576 (2013) 350-357.
- [27] S. Najafi, A.R. Eivani, M. Samaee, H.R. Jafarian, J. Zhou, A comprehensive investigation of the strengthening effects of dislocations, texture and low and high angle grain boundaries in ultrafine grained AA6063 aluminum alloy, *Materials Characterization* 136 (2018) 60-68.
- [28] E.A. El-Danaf, Mechanical properties, microstructure and texture of single pass equal channel angular pressed 1050, 5083, 6082 and 7010 aluminum alloys with different dies, *Materials & Design* 32(7) (2011) 3838-3853.
- [29] C. Pithan, T. Hashimoto, M. Kawazoe, J. Nagahora, K. Higashi, Microstructure and texture evolution in ECAE processed A5056, *Materials Science and Engineering: A* 280(1) (2000) 62-68.
- [30] Q. Jining, J.-H. Han, Z. Guoding, J.-C. Lee, Characteristic of textures evolution induced by equal channel angular pressing in 6061 aluminum sheets, *Scripta Materialia* 51(2) (2004) 185-189.
- [31] S. Suwas, R. Arruffat-Massion, L.S. Tóth, A. Eberhardt, J.-J. Fundenberger, W. Skrotzki, Evolution of crystallographic texture during equal channel angular extrusion of copper: The role of material variables, *Metallurgical and Materials Transactions A* 37(3) (2006) 739-753.
- [32] W.H. Huang, L. Chang, P.W. Kao, C.P. Chang, Effect of die angle on the deformation texture of copper processed by equal channel angular extrusion, *Materials Science and Engineering: A* 307(1-2) (2001) 113-118.
- [33] S. Li, A.A. Gazder, I.J. Beyerlein, C.H.J. Davies, E.V. Pereloma, Microstructure and texture evolution during equal channel angular extrusion of interstitial-free steel: Effects of die angle and processing route, *Acta Materialia* 55(3) (2007) 1017-1032.
- [34] I.J. Beyerlein, L.S. Tóth, Texture evolution in equal-channel angular extrusion, *Progress in Materials Science* 54(4) (2009) 427-510.
- [35] L.S. Tóth, Texture Evolution in Severe Plastic Deformation by Equal Channel Angular Extrusion, *Advanced Engineering Materials* 5(5) (2003) 308-316.
- [36] S.C. Baik, Y. Estrin, R.J. Hellmig, H.-T. Jeong, H.G. Brokmeier, H.S. Kim, Modeling of texture evolution in copper under equal channel angular pressing, *Zeitschrift für Metallkunde* 94(11) (2003) 1189-1198.
- [37] S. Suwas, L.S. Tóth, J.-J. Fundenberger, A. Eberhardt, W. Skrotzki, Evolution of crystallographic texture during equal channel angular extrusion of silver, *Scripta Materialia* 49(12) (2003) 1203-1208.
- [38] I.J. Beyerlein, R.A. Lebensohn, C.N. Tomé, Modeling texture and microstructural evolution in the equal channel angular extrusion process, *Materials Science and Engineering: A* 345(1-2) (2003) 122-138.
- [39] G. Purcek, B.S. Altan, I. Miskioglu, P.H. Ooi, Processing of eutectic Zn-5% Al alloy by equal-channel angular pressing, *Journal of Materials Processing Technology* 148(3) (2004) 279-287.
- [40] P. Kumar, C. Xu, T.G. Langdon, Mechanical characteristics of a Zn-22% Al alloy processed to very high strains by ECAP, *Materials Science and Engineering: A* 429(1-2) (2006) 324-328.

- [41] G. Purcek, O. Saray, I. Karaman, M. Haouaoui, Microstructural Evolution and Mechanical Response of Equal-Channel Angular Extrusion-Processed Al-40Zn-2Cu Alloy, *Metallurgical and Materials Transactions A* 40(11) (2009) 2772.
- [42] H.L. Jia, R. Bjørge, K. Marthinsen, R.H. Mathiesen, Y.J. Li, Soft particles assisted grain refinement and strengthening of an Al-Bi-Zn alloy subjected to ECAP, *Materials Science and Engineering: A* 703 (2017) 304-313.
- [43] Y. Iwahashi, Z. Horita, M. Nemoto, T.G. Langdon, Factors influencing the equilibrium grain size in equal-channel angular pressing: Role of Mg additions to aluminum, *Metallurgical and Materials Transactions A* 29(10) (1998) 2503-2510.
- [44] G.R. Canova, U.F. Kocks, J.J. Jonas, Theory of torsion texture development, *Acta Metallurgica* 32(2) (1984) 211-226.
- [45] E.A. El-Danaf, M.S. Soliman, A.A. Almajd, EBSD investigation of the microstructure and microtexture evolution of 1050 aluminum cross deformed from ECAP to plane strain compression, *Journal of Materials Science* 46(10) (2011) 3291-3308.